Sensors and Materials, Vol. 38, No. 7 (2026) 4049–4068
MYU Tokyo

S & M 4549

Design and Experimental Validation of a Multi-output Power Management Unit for a Multiple-particles Analyzer under Dynamic-load and Thermal-vacuum Conditions

Yung-Tsung Cheng,[1] Tzu-Fang Chang,[2*] Chih-Yu Chiang,[2]
Yu-Rong Cheng,[3] and Cheng-Chi Tai[3]

[1]Department of Electric Vehicles and Intelligent Electronics, Kun Shan University,
No. 195, Kunda Rd., Yongkang Dist., Tainan 71003, Taiwan
[2]Institute of Space and Plasma Sciences, National Cheng Kung University,
No. 1, University Road, Tainan 70101, Taiwan
[3]Department of Electrical Engineering, National Cheng Kung University,
No. 1, University Road, Tainan 70101, Taiwan

(Received November 18, 2025; accepted July 10, 2026)

Keywords: power management unit, multiple-particles analyzer, thermal-vacuum chamber testing, spaceborne power electronics

The rapid development of CubeSat-class missions has markedly increased the demand for high-efficiency and highly reliable power management systems capable of operating in the harsh space environment. In this study, we validated a highly integrated, multi-output power management unit (PMU) designed for a multiple-particles analyzer (MPA) developed under CubeSat-class specifications. The proposed PMU provides both isolated and non-isolated stable output rails from input buses of ±15 and +5 V. The system incorporates inrush-current suppression, electronic fuse (e-Fuse) protection, and real-time voltage, current, and temperature monitoring functions to ensure operational safety and reliability. In both static- and dynamic-load tests, the developed PMU demonstrated excellent steady-state stability, with measured ripple voltages of 63 mVpp (1.05%) for the +6 V rail and 46 mVpp (0.77%) for the −6 V rail, meeting the MPA's power-quality requirements. During dynamic-load changes from 80 to 10 mA, the +6 V rail exhibited an overshoot of approximately 120 mV that recovered within 2 μs, confirming the effectiveness of the compensation and recovery network. The peak inrush currents for all input rails remained below 420 mA, confirming the stability and robustness of the circuits for controlling the inrush current. The thermal-vacuum simulation tests further confirmed the PMU's environmental robustness: across a temperature range from −40 to +70 °C, the unit maintained voltage regulation without observable drift, demonstrating strong thermal stability and suitability for the space environment. The overall experimental results confirm that the proposed PMU achieves both electrical stability and environmental robustness, and therefore represents a lightweight, modular, and highly integrated power solution for the MPA. Moreover, this design provides a foundation for future developments aimed at increased

*Corresponding author: e-mail: jocelyn@pssc.ncku.edu.tw
https://doi.org/10.18494/SAM6042

ISSN 0914-4935
https://myukk.org/

power densities and long-duration mission operations in space applications. Beyond power conversion, the PMU embeds on-board voltage, current, and temperature sensing for real-time health monitoring; this integrated telemetry not only safeguards the particle-sensing MPA payload but also provides a continuous data stream that can underpin Artificial Intelligence of Things (AIoT) and intelligent-sensing functions such as autonomous fault diagnosis and predictive maintenance. The PMU integrates on-board temperature (MCP9700) and voltage/current sensing for real-time health monitoring, and its thermal behavior was further characterized through multi-point temperature sensing during thermal-vacuum testing. As the enabling and protection unit for the MPA—a particle-sensing payload—the PMU, together with the payload, was additionally subjected to proton single-event-effect and ^{60}Co total-ionizing-dose radiation testing to verify its reliability in the space environment.

1. Introduction

The microsatellite market has recently experienced rapid growth. Microsatellites offer advantages over traditional large-scale satellites such as being compact, lightweight, and inexpensive, and having short development cycles. These characteristics have enabled the diversity of national research institutions, academic organizations, and private enterprises to actively participate in satellite development. To further reduce design and launch barriers, the CubeSat-class standard was proposed by California Polytechnic State University in 1999,(1) in which a single satellite unit was defined as a 10 × 10 × 10 cm^3 cube with a maximum mass of 1.33 kg. The establishment of this standard markedly reduced the technological requirements for launch, facilitating global standardization and the widespread adoption of CubeSat-class missions.(2,3) Both research and in-orbit mission verifications of the CubeSat-class platform performed in Taiwan have demonstrated its feasibility for conducting scientific experiments and educational applications under specific resource constraints.(4) Ongoing expansions of CubeSat-class missions in both complexity and scope have increased the importance of the design of the electrical power system (EPS). According to previous studies, small-satellite power systems can generally be divided into three major subsystems: energy generation, energy storage, and energy distribution. Among them, the power management unit (PMU) plays a key role in energy distribution—it must not only provide stable power outputs but also simultaneously exhibit high power density, electromagnetic compatibility (EMC), reliability, and low power consumption. Previous research has primarily focused on the energy generation aspect of CubeSat-class systems. For example, Lotfy *et al.*(5) analyzed the effects of photovoltaic systems and electric propulsion on satellite life span, and highlighted the critical impact of energy generation on overall mission sustainability.

However, beyond energy generation and storage, efficiently distributing the fixed electrical power to multiple payloads and subsystems remains a core challenge for ensuring mission success. Existing satellite power technologies still exhibit notable limitations. For example, the National Aeronautics and Space Administration (NASA)'s Small Spacecraft Technology State-of-the-Art reports published in 2021 and 2024(6,7) indicated that while considerable progress has been made in power generation and storage, payload-oriented PMUs still face bottlenecks in multi-output integration, inrush-current suppression, and health-monitoring functionality. Several recent studies have proposed modular PMU architectures tailored for CubeSat-class applications[8–10] that improve both efficiency and space utilization. Shakoor *et al.*[11] reviewed the current development trends of CubeSat-class EPS and emphasized the importance of standardizing EPS architectures, but they did not perform a detailed experimental validation of payload-oriented PMU designs. Regarding reliability, Aburouk *et al.*[12] proposed a reliability-oriented DC/DC converter design for low-Earth-orbit missions; however, their validation was restricted to single-module evaluations, and so they did not assess intermodule integration. Chacón *et al.*[13] presented several mitigation strategies for inrush-current suppression, which were primarily designed for large-scale aerospace power systems, and so left CubeSat-class PMU implementations underexplored. Moreover, Cervone *et al.*[14] and Bouwmeester *et al.*[15] highlighted the importance of incorporating health monitoring and fault-tolerant mechanisms into CubeSat-class power systems to improve the mission life span, but practical implementations and verifications remain scarce. PMU designs must also undergo the verification of their environmental robustness, particularly through thermal-vacuum chamber (TVC) testing,[16–19] to ensure operational reliability under the extreme temperature and pressure conditions typical of the space environment.

In this study, we addressed the above-mentioned research gaps and technical challenges by designing and constructing a compact, highly integrated multi-output PMU for the multiple-particles analyzer (MPA) payload. The PMU was designed to meet stringent constraints on size, mass, power consumption, and EMC imposed by the CubeSat-class platform. It operates from ±15 V/0.2 A and +5 V/1.5 A input buses and provides multiple regulated output rails—including isolated ±12 V rails—and integrates inrush-current suppression, electronic fuse (e-Fuse) protection, and real-time voltage, current, and temperature monitoring. We particularly focused on effective inrush-current suppression and low-power operation, both of which are critical to ensuring system stability and extending mission life span. Through empirical design and validation, we aimed to provide a fully verified PMU solution for the MPA payload and provided a foundation for future radiation-tolerance and long-term reliability assessments in CubeSat-class spacecraft. In this respect, the proposed PMU is a power converter with integrated sensing telemetry: its built-in voltage, current, and temperature sensing channels generate the telemetry required for the on-board health management of the MPA particle-sensing payload. This places the present work within the scope of physical-sensor and intelligent-sensing applications, since the same monitoring data can serve as the input layer for AIoT-oriented diagnostic and adaptive power-management schemes. The main contribution of this work is therefore not the individual building blocks—soft-start, e-Fuse protection, monitoring circuits, and DC/DC conversion are all established techniques—but the integration of these mature techniques, drawn from different application domains, into a single compact, multi-output, isolated, and health-monitored payload PMU, and the validation of that integration under the stringent and largely non-adjustable electrical and environmental constraints of the space environment through a complete electrical, thermal-vacuum, and preliminary radiation test methodology.

2. Materials and Methods

2.1 Design specifications and system interface

The PMU was designed and implemented in strict accordance with the CubeSat Design Specification(1) and the electrical interface requirements of the MPA payload. According to the MPA mission's power-on sequence plan, the maximum input bus to the PMU is defined as ±15 V (with current limits of 0.2 A for both the positive and negative buses) and +5 V (with a current limit of 1.5 A). Accordingly, the design objective of the present PMU was to provide multiple regulated outputs within a compact form factor to meet the electrical requirements of the various sensors and electronic components of the MPA.

The primary output specifications in terms of the required PMU input/output specifications, performance targets, and protection functions are summarized in Table 1, which were designed to ensure system reliability and conform with both the design constraints and performance objectives. FS-8C is one satellite of the Formosat-8 (FS-8) constellation, Taiwan's first domestically developed remote-sensing satellite constellation, which comprises eight optical remote-sensing satellites to be deployed incrementally into a 561 km Sun-synchronous orbit and operated as a self-owned Earth-observation system. These requirements were directly derived from the Formosat-8C (FS-8C) spacecraft power management allocation guidelines, while the design goals focused on high efficiency, operational reliability, and compatibility with the MPA mission's power-distribution architecture.

2.2 Inrush-current suppression principle and strategy

The inrush current (i_{inrush}) refers to the transient surge of current that occurs at the instant when the PMU is first powered on. At power-on, the input current charges the input capacitor

Table 1
System input and output specifications and design targets.

Parameter	Specification	Design target
Bus inrush currents	+15 V/0.5 A, −15 V/0.4 A, +5 V/2.5 A	Complies with the transient power-supply limitations of the main system during the subsystem power-on phase to prevent damage to sensitive electronic components from large transient currents
Bus steady-state currents	±15 V/0.2 A, +5 V/1.5 A	Complies with the long-term power-supply allocation strategy of the parent system under steady-state operation
Output rails	+5 V non-isolated, ±6 V non-isolated, ±12 V non-isolated, ±12 V isolated; all ±2%	Provides multiple independent output rails, supporting digital/analog loads and isolation requirements
Average power	<2 W	Meets the low-power requirements in the energy-constrained environment of CubeSat-class systems
Protection	Positive and negative voltage surge control, e-Fuse	Improves power-on and operational reliability to prevent short-circuit and overcurrent damage
Monitoring	Current and temperature monitoring	Provides real-time voltage, current, power, and temperature monitoring, supporting health management and fault prevention

(C_{in}) of the DC/DC converter, resulting in a short-duration, high-amplitude current. The magnitude of this transient current can be several times higher than that observed under steady-state operation. This phenomenon may inadvertently trigger the protection circuits of the FS-8C or the spacecraft's power distribution unit, potentially causing component degradation, compromising system stability, or shortening the overall life span of the payload subsystem. Therefore, the electrical operation of the entire system must be evaluated comprehensively during the early design phase, and appropriate countermeasures must be implemented to limit the inrush current. The inrush current can be expressed as

$$i_{inrush}(t) = \frac{V_{in}}{R_{eq}} e^{-\frac{t}{R_{eq}C_{in}}}, \tag{1}$$

where V_{in} denotes the input voltage and R_{eq} represents the equivalent series resistance of the system, which includes the wiring resistance, the current-limiting resistor, and the equivalent series resistance of the input capacitors. To ensure that both the peak amplitude of the inrush current (i_{peak}) and its duration ($T_{duration}$) comply with system-level requirements, the PMU applies an active suppression strategy that combines instantaneous current monitoring with a soft-start mechanism. This mechanism gradually increases the gate drive signal immediately after power-on, effectively limiting i_{peak} while extending $T_{duration}$. By controlling the rate of the voltage increase across the converter input stage, the soft-start circuit ensures that the input capacitors are charged smoothly, which prevents the false triggering of the upstream protection circuits and ensures full compliance with the FS-8C electrical interface specifications.

3. System Architecture and Design

The system was designed while considering the stringent constraints and challenges imposed by the MPA in terms of size, power, and operational environment. To ensure long-term stability and autonomous monitoring capability, the PMU was designed as a highly integrated system that consolidates multiple functional modules, enabling comprehensive power management through both active and passive monitoring mechanisms, as illustrated in Fig. 1. The integrated modules include the inrush-current management module that is responsible for limiting transient current surges during power-on; the e-Fuse, which provides overcurrent protection and fault isolation; the voltage and current monitoring module, which is used for real-time telemetry and feedback control; the temperature sensing module, which provides thermal protection and environmental tracking; and the DC/DC and isolated DC converter circuits, which generate regulated output voltage rails that will be supplied to different payload subsystems. These modules together form a unified architecture that enables the PMU to achieve reliable, efficient, and intelligent power distribution for CubeSat-class payload applications.

The inrush-current management module employs the LT4356 and LM5068 controllers (Analog Devices and Texas Instruments), which plays a critical role during system power-on. Its primary function is to monitor and limit transient current surges to ensure that the inrush current

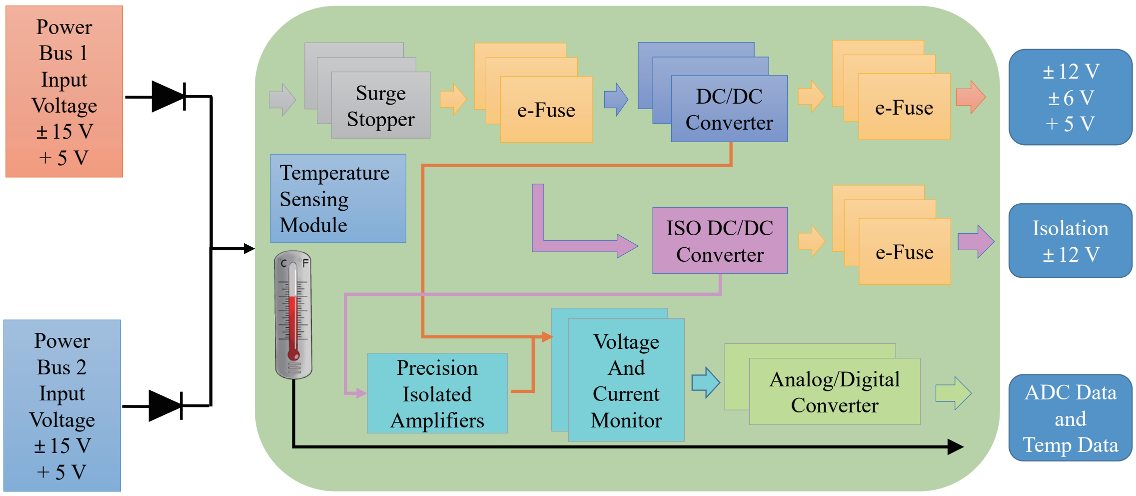

Fig. 1. (Color online) System architecture.

does not exceed a predefined safety threshold. This design is effective at protecting downstream circuits and sensitive components from large current spikes during power-on. The stability of this module is of paramount importance for CubeSat-class systems, since they are characterized by low power budgets and high sensitivity to current fluctuations. The e-Fuse utilizes the TPS26602 device (Texas Instruments) to provide instantaneous overcurrent protection. It continuously monitors the operating current of each output rail and immediately disconnects the power supply if an overcurrent or short-circuit condition is detected. Its rapid-isolation characteristic stops faults from propagating to other subsystems, thereby improving the overall system reliability and operational safety. The voltage and current monitoring module includes an INA146 precision amplifier (Texas Instruments) that accurately records the power consumption in various operating modes. These data are essential for evaluating system efficiency, optimizing energy utilization strategies, and performing fault diagnosis and health monitoring. The temperature sensing module employs the MCP9700 device (Microchip Technology) to enable the real-time temperature monitoring of the PMU and nearby critical components. The acquired temperature data are transmitted to the main system for logging and analysis. In the harsh thermal environment of space, this function is vital for preventing component degradation caused by overheating or excessive cooling, and it provides valuable input for refining thermal management strategies. Finally, the DC/DC converter circuits are implemented with the TPS54540 (Texas Instruments) and LT3094 (Analog Devices) devices together with the isolated DC converter module (MAEU02-HI, MINMAX), and they serve as the core energy conversion units of the PMU. These converters regulate the electrical power supplied by the FS-8C main bus into multiple stable voltage and current outputs required by the MPA subsystems. The isolated DC/DC converter enables galvanic isolation between the source and the load, which suppresses conducted noise/emissions and improves the overall EMC and noise immunity of the system. This ensures the integrity and reliability of scientific data collected by the MPA payload.

4. Results

A drawing of the prototype multifunctional PMU system board is provided in Fig. 2(a), while a photograph of the actual hardware implementation is shown in Fig. 2(b). The power input is interfaced via a DB15 connector located at the upper-right corner of the board. The output rails and signal terminals are routed via connectors positioned along the left and lower-right sections of the PCB, providing convenient access for system integration and the testing of channels.

A Prodigit 3311F electronic load tester was used to conduct both static- and dynamic-load tests, with an Agilent DSO9064A digital oscilloscope employed to analyze the voltage waveforms. In addition, an Agilent N2782A current probe was used to measure the inrush current, as illustrated in Fig. 2(c). These tests were designed to emulate the actual operational conditions of the PMU when connected to the corresponding payload circuits and powered by the satellite bus. The measured parameters—output voltage, output current, and inrush current—were compared with the design specifications to verify the compliance of the PMU and that it was stable under varying load conditions. Finally, the PMU was installed in a TVC to perform a thermal-vacuum cycling test, as shown in Fig. 2(d). This test simulated temperature variations that are typically encountered in the space environment, with the objective of ensuring

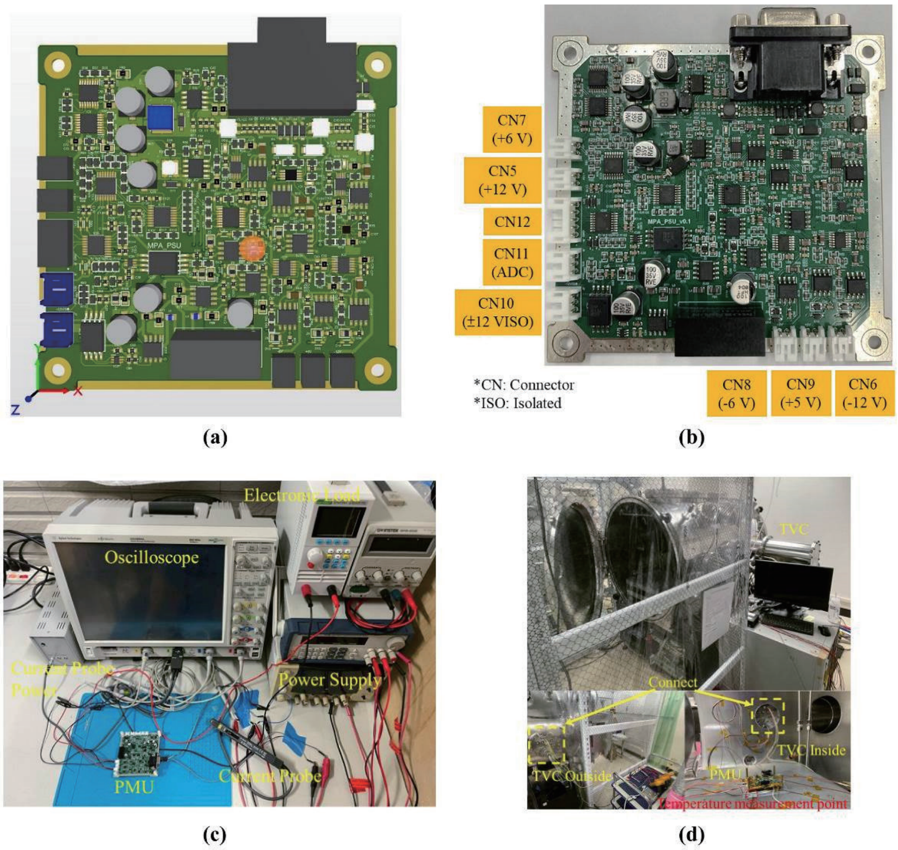

Fig. 2. (Color online) Multi-functional PMU PCB: (a) drawing and (b) photograph of the actual hardware implementation. (c) Experimental setup for static- and dynamic-load measurements. (d) TVC setup.

that the PMU can operate stably and provide its regulated outputs under extreme thermal conditions.

The PMU's overall power consumption and physical characteristics were also characterized to support the low-powers and compact design objectives. Under nominal operating conditions, the measured input power drawn from the three supply buses were 0.75 W (+15 V at 50 mA), 0.675 W (−15 V at 45 mA), and 0.50 W (+5 V at 100 mA), giving a total average input power of approximately 1.93 W, which meets the <2 W design target listed in Table 1. The assembled PMU board measures 91.9 × 93.0 × 14 mm^3 with a mass of 113 g, confirming its suitability for the volume and mass budgets of CubeSat-class payloads. Because the present test campaign used the nominal MPA operating point rather than a controlled per-rail load sweep, we report nominal input power instead of claiming per-rail efficiency; a complete per-rail conversion-efficiency characterization across the full load range is identified as future work.

4.1 Static-load test

A static-load power-on test was first conducted to evaluate the output stability of the system under fixed-load current conditions and to verify the response of the e-Fuse protection mechanism, as shown in Fig. 3. The experimental results show that setting the load to 80 mA resulted in a transient inrush current of approximately 108 mA in the +6 V rail at power-on, which momentarily triggered the e-Fuse protection circuit. However, the system successfully entered the fault-recovery mode and subsequently maintained a stable output voltage. Increasing the load to 90 mA resulted in the power-on current continuously exceeding the e-Fuse's preset current threshold (designed at approximately 85 mA), causing the system to exhibit cyclic restarts (hiccup mode) as it repeatedly attempted to re-establish output regulation; the system was ultimately unable to reach a steady-state output under this condition. These observations confirm that, under static conditions, the e-Fuse provides effective protection by strictly limiting the output current, thereby preventing excessive loading. However, they also indicate that the

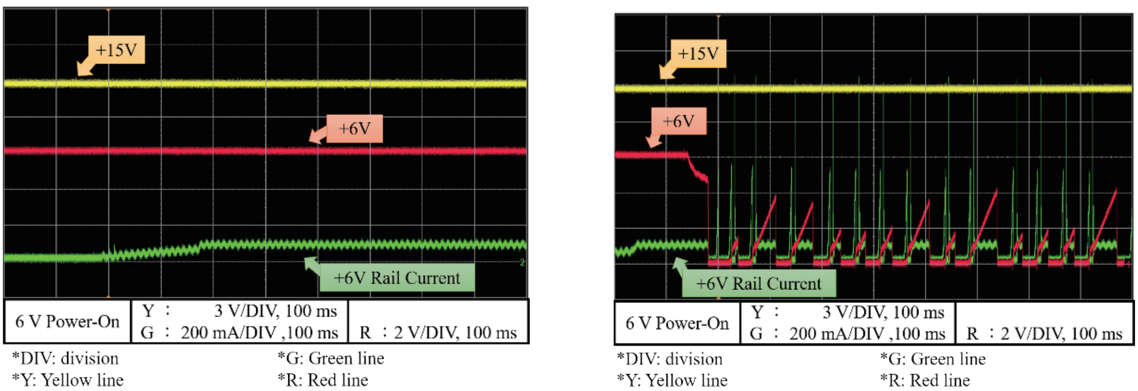

(a) (b)

Fig. 3. (Color online) Voltage static-load experimental results for the +6 V rail at loads of (a) 80 and (b) 90 mA.

design margin of the output rail during static power-on was relatively narrow, suggesting the need for further optimization of the protection threshold and coordination of the soft-start mechanism.

4.2 Dynamic-load test

A dynamic-load test was conducted to evaluate the output stability of the PMU under sudden load transients that simulated the rapid current fluctuations that may occur in the MPA payload system when the particle detector and signal acquisition boards respond to incident particles. During testing, a load step-down condition was applied to the ±6 V rails by instantaneously switching the load current from 80 to 10 mA. As shown in Fig. 4, under steady-state conditions, the peak-to-peak output ripple voltage measured approximately 63 mV (1.05%) for the +6 V rail and 46 mV (0.77%) for the −6 V rail. According to previous studies,[9,10] it is typically recommended that CubeSat-class power systems ensure that the output ripple does not exceed 2% of the nominal voltage. Therefore, the measured ripple voltages of this PMU complied with this standard, confirming its excellent filtering performance and high output stability during steady-state operation. At the moment when the load step-down was applied, a transient voltage overshoot and high-frequency ringing phenomena were observed on both output rails. For the +6 V rail, the overshoot amplitude was approximately 120 mV (2.0%), with a rapid recovery time of about 2 µs. These transient characteristics are typical behaviors of switched-mode power converters and primarily originate from electromagnetic resonances caused by parasitic inductance and capacitance in the circuits. Given that the magnitude of the voltage change and the short transient recovery time are well within the MPA system's hold-up time tolerance, the experimental results confirm that the ±6 V rails exhibited stable and reliable performance under dynamic-load conditions, fully satisfying the MPA payload's stringent requirements for high signal integrity and electrical reliability.

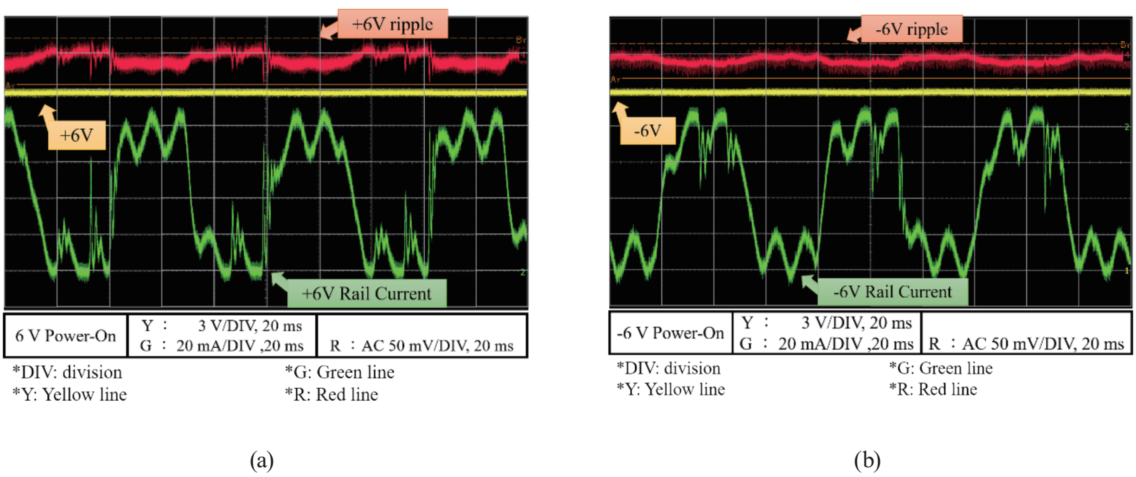

Fig. 4. (Color online) Measured waveforms of ±6 V rails under dynamic-load and ripple-voltage testing: (a) +6 and (b) −6 V rails.

4.3 Inrush-current measurements

The inrush-current suppression performance of the PMU was experimentally verified by precisely measuring the peak inrush currents on the ±15 and +5 V input buses. The +15 V bus exhibited a multi-peak current waveform during power-on, with a peak current of approximately 360 mA. The −15 V bus recorded a peak of 360 mA, while the +5 V bus peaked at almost 420 mA. Among the input buses, the −15 V bus exhibited the smallest margin relative to its transient limit (about 360 mA against a 400 mA limit). This is because the −15 V bus—supplied directly by the host spacecraft—simultaneously feeds both the −6 V rail, generated by an LT3094 negative-voltage low-dropout regulator, and the isolated DC/DC module; at power-on, this single bus must charge the input and output capacitances of these multiple downstream stages together with the start-up behavior of the negative-rail regulation, resulting in a slightly higher peak inrush relative to its limit. The measured ~360 mA nevertheless remains safely below the 400 mA transient limit of the FS-8C bus, and this margin can be further increased by staggering the power-on sequence or tuning the soft-start of the downstream stages if required. Since all measured peak inrush currents (<420 mA) were well below the transient current limits defined for the FS-8C power bus, as specified in Table 1, these results strongly support the effectiveness of the PMU's inrush-current suppression circuit. The design successfully ensures that powering on the system does not trigger the undervoltage or overcurrent protection mechanism of the FS-8C power-distribution system. However, the power-on fault tolerance can be improved by the future optimization of the inrush-current suppression circuit parameters. By fine-tuning the control thresholds and timing constants within the transient limit of the power bus—without compromising the operational stability or scientific performance of the MPA—the system can exhibit a larger design safety margin that will reduce the risk of false triggering of the spacecraft's protection circuit.

Figure 5(a) presents the complete measured waveform of the +15 V bus during power-on, whereas Fig. 5(b) shows a zoomed-in view of the inrush-current waveform. The first inrush-

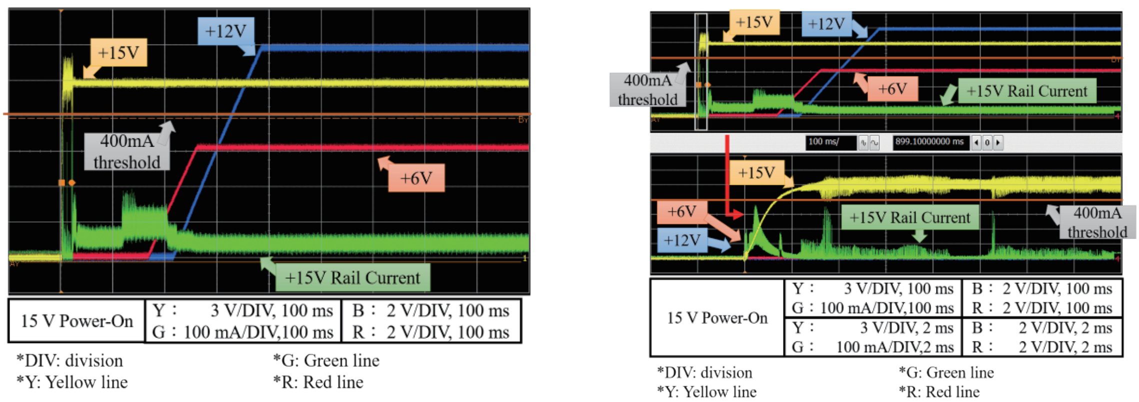

(a) (b)

Fig. 5. (Color online) Inrush-current measurements, with each rail and the corresponding bus current labeled directly on the waveforms: (a) powering on the +15 V bus and (b) zoomed-in view of the inrush current.

current peak reached approximately 360 mA, followed by successive peaks of 350 and 330 mA. After these transient surges, the output voltage successfully stabilized at the correct value. These measured results are consistent with the design specifications, confirming that the inrush-current suppression circuit is effective at regulating the transient current behavior during power-on and ensures reliable voltage ramp-up without exceeding the defined safety thresholds.

Figure 6(a) shows the complete measured waveform of the −15 V bus during power-on, whereas Fig. 6(b) presents a zoomed-in view of the inrush-current behavior. The first inrush-current peak was approximately 80 mA, followed by a second peak at 90 mA and a third peak reaching about 360 mA. After these transient surges, the output voltage successfully stabilized at the correct value. The measured waveform was closely aligned with the design specifications, demonstrating that the inrush-current suppression circuit is effective at managing the transient behavior during power-on and ensures the reliable establishment of the specified voltage within the defined safety and performance criteria.

Figure 7(a) illustrates the complete measured waveform of the +5 V bus during power-on, whereas Fig. 7(b) presents a zoomed-in view of the inrush-current waveform. The inrush current

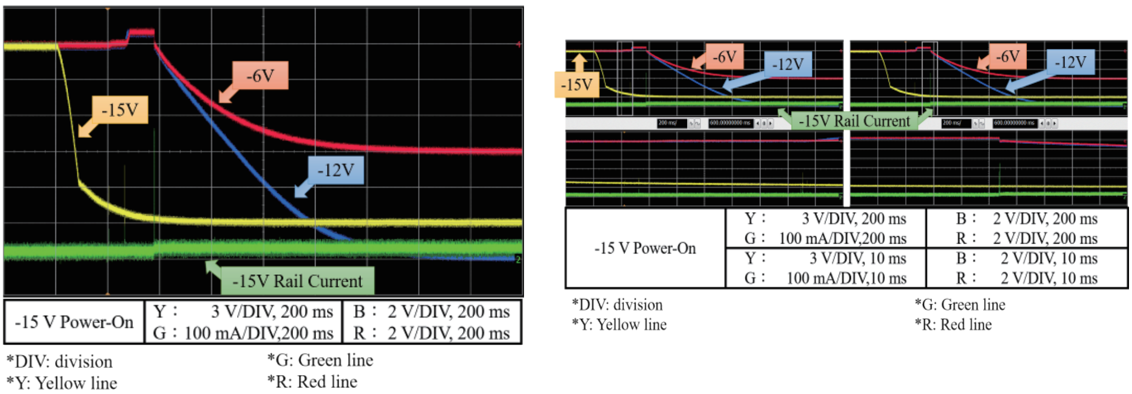

(a) (b)

Fig. 6. (Color online) Inrush-current measurements, with each rail and the corresponding bus current labeled directly on the waveforms: (a) powering on the –15 V bus and (b) zoomed-in view of the inrush current.

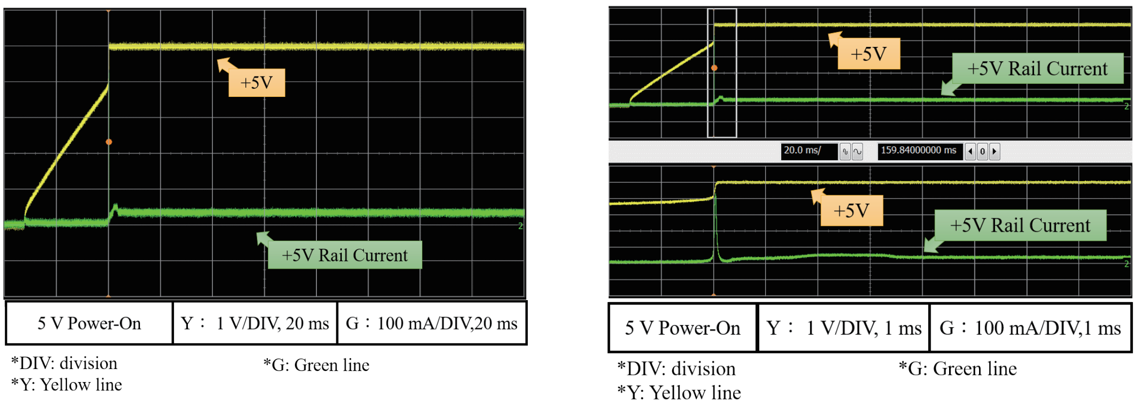

(a) (b)

Fig. 7. (Color online) Inrush-current measurements: (a) powering on the DC +5 V bus and (b) zoomed-in view of the inrush current.

reached a peak of approximately 420 mA before the output voltage successfully stabilized at the correct value. The measured results are in full compliance with the design specifications, confirming that the inrush-current suppression circuit operates effectively and ensures a controlled power-on sequence within the defined safety margins.

4.4 Temperature measurements in a simulated space environment in the TVC

The thermal stability and reliability of the designed PMU in a simulated space environment were verified by conducting simulation experiments in a TVC. The chamber was maintained at a vacuum of 10^{-6}–10^{-7} torr, and the temperature was cycled from −40 to +70 ℃. The temperature was ramped at 1 ℃ per min, with a 60 min dwell period at each extreme temperature. Three temperature sensing points were configured inside the chamber using thermocouples [Fig. 8(a)]: T1 was positioned inside the chamber to monitor the ambient reference temperature, T2 was at the metallic mounting base of the PMU, and T3 was at the PMU PCB near the secondary regulation circuit. The output voltages were measured externally to prevent the thermal environment from interfering with the measurement circuits. As shown in Fig. 8(b), the output voltage remained highly stable throughout the temperature cycling process. Across all output rails, the voltage deviation ranged from approximately 0 to 30 mV (0 to 0.75%) at −40 ℃ and from approximately 0 to 40 mV (0 to 0.82%) at +70 ℃, corresponding to a mean absolute deviation of about 0.2%, confirming excellent thermal stability, with all non-isolated rails within ±1%. The temperature measurements further revealed that when the chamber reached the extremes of −40 and +70 ℃, the actual PMU temperatures were approximately −15 and +50 ℃, respectively. These discrepancies are attributable to limitations in thermal conductivity between the PMU and the metallic base plate, which were fastened together using brass standoffs.

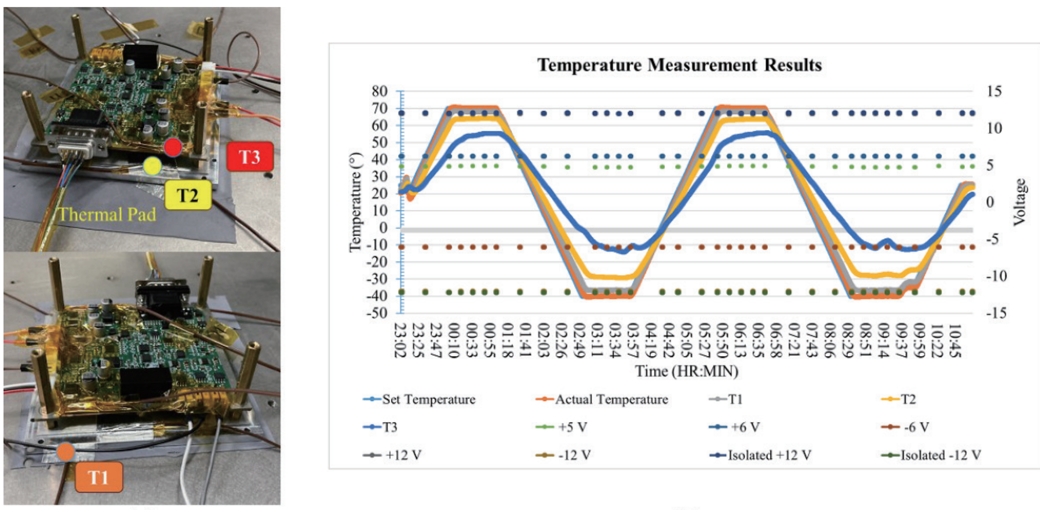

(a) (b)

Fig. 8. (Color online) Temperature measurements in the TVC: (a) PMU temperature measurement points and (b) measured temperatures and output voltages.

Overall, no marked voltage drifts or oscillations were observed during the temperature cycling process, indicating that the PMU's voltage regulation loop exhibited excellent thermal stability. Moreover, no transient disturbances induced by the vacuum environment were detected, demonstrating that the control compensation network and component selection effectively mitigated the effects of thermal stress on the converter circuitry. Collectively, these results confirm that the proposed PMU can provide stable output voltages across a wide temperature range and under radiative heat dissipation conditions, thereby validating its environmental robustness and engineering feasibility in space applications.

The experimental results confirm that the proposed PMU exhibits stable performance in terms of multiple regulated output rails, dynamic-load response, inrush-current suppression, and thermal-vacuum temperature cycling, and hence fulfills the core operational requirements of satellite payload subsystems. However, the results also reveal opportunities for further improvement under high-load power-on conditions and for negative voltage inputs, where additional circuit optimization can improve the power-on reliability and voltage stability. Similarly, the duration and number of thermal-vacuum cycles can be refined in future testing to more fully assess the long-term thermal endurance and material properties. Such additional experimental data will not only further verify the feasibility of the proposed PMU design but also provide a solid empirical foundation for subsequent refinements aimed at improving the overall system reliability and environmental robustness in future space missions.

4.5 Radiation test results

To assess the tolerance of the payload electronics to the space radiation environment, single-event effect (SEE) and total-ionizing-dose (TID) tests were performed on the MPA payload, which includes the PMU board. In both tests, the payload was continuously operated and monitored, and functional/performance checks were carried out before and after irradiation to confirm that the radiation exposure did not degrade its operation.

The SEE test was conducted using a 200 MeV proton beam at a flux of 2.25×10^7 particles/ cm^2/s, reaching a total fluence of 8.73×10^{10} particles/cm^2 and an accumulated dose of approximately 5 krad (50 Gy) over a maximum scan area of 29.6×24.5 cm^2. The exposure was applied over about 66 beam cycles (60 s beam-on followed by ~55 s beam-off per cycle), with an acceptance tolerance of 0 to +10%. Throughout the entire SEE test, the payload continued to operate normally, with no system latch-up, crash, or unexpected reboot observed, indicating robustness against single-event-induced upsets under the tested conditions.

The TID test used a ^{60}Co gamma source to a target accumulated dose of 10 krad (100 Gy). The payload was placed 40 cm in front of the source so that the beam covered the entire unit; at the corresponding dose rate of 28 Gy/h at 40 cm, the 10 krad target was reached in approximately 4 h. Pre- and post-irradiation functional and performance tests confirmed that the payload operated normally after exposure, again with no crash or reboot observed, indicating that the accumulated ionizing dose did not impair its function within the tested range.

These results provide initial experimental evidence of radiation tolerance for the payload electronics, including the PMU, under the tested proton-SEE and ^{60}Co-TID conditions, as summarized in Table 2. Comprehensive flight-level radiation qualification—covering a wider range of devices, higher accumulated doses, and heavy-ion SEE characterization—remains as future work.

5. Discussion

The comprehensive experimental validation performed in this study has confirmed that the proposed PMU demonstrates excellent performance in terms of functional integration, output stability, and environmental robustness, as summarized in Table 3. The results from both the static- and dynamic-load tests indicate that the PMU provided multiple stable regulated output rails under both steady-state and transient conditions. The measured output ripple voltages were 63 mV for the +6 V rail and 46 mV for the −6 V rail, which are both within the typically recommended 2% tolerance range for CubeSat-class power systems, verifying the effectiveness of the compensation network and output filter design. Furthermore, the observed transient overshoot of approximately 120 mV with a recovery time of about 2 μs reflects a sufficient phase margin and control-loop stability, ensuring the reliable operation of the payload even under rapid load changes. During inrush-current testing, the input protection circuits—comprising a LT4356 controller, a LM5068 controller, and TPS26602 e-Fuse—effectively restricted the peak inrush current to <420 mA, confirming that the combined soft-start and staged activation strategy successfully balances the power-on speed and component protection. Although multiple current peaks were observed during power-on, they were attributed to asynchronous charging among

Table 2
Radiation test conditions and results for the MPA payload (including the PMU).

Parameter	SEE test	TID test
Source	200 MeV proton beam	^{60}Co gamma
Flux / dose rate	2.25×10^7 particles/cm^2/s	28 Gy/h at 40 cm
Total fluence	8.73×10^{10} particles/cm^2	—
Accumulated dose	≈5 krad (50 Gy)	10 krad (100 Gy), ≈4 h
Exposure profile	≈66 cycles (60 s on / ~55 s off)	Continuous
Acceptance tolerance	0 to +10%	Pre/post-functional test
Result	Normal; no latch-up/crash/reboot	Normal; no crash/reboot

Table 3
Summary of measured PMU performance against design requirements.

Test	Measured result	Requirement/remark
Steady-state ripple (+6 V)	63 mV_{pp} (1.05%)	≤2% of nominal — pass
Steady-state ripple (−6 V)	46 mV_{pp} (0.77%)	≤2% of nominal — pass
Dynamic-load overshoot (+6 V)	≈120 mV (2.0%), recovery ≈2 μs	Within MPA hold-up tolerance
Peak inrush, +15 V bus	≈360 mA	<500 mA limit — pass
Peak inrush, −15 V bus	≈360 mA	<400 mA limit — pass (smallest margin)
Peak inrush, +5 V bus	≈420 mA	<2.5 A limit — pass
Thermal-vacuum stability (−40 to +70 °C)	Output deviation ≤±1%	No observable drift or oscillation
Average input power	≈1.93 W	<2 W target — pass

multiple input capacitors and the timing sequence of the protection circuits. The future optimization of the output rail power-on delay and precharge control parameters can further reduce the bus voltage stress and improve the behavior during a cold start, including reducing the hiccup mode.

Thermal-vacuum testing further validated the reliability of the PMU under extreme temperature and low-pressure conditions. Within the −40 to +70 ℃ range of temperature cycling, the deviations in output rail voltages remained within ±1%, confirming stable performance under radiative heat dissipation and thermal gradient conditions. The temperature measurements revealed a thermal discrepancy of approximately 20 ℃ between the mounting base and the PCB surface (sensing points T2 and T3, respectively), primarily due to limitations in the thermal conductivity of the brass standoffs used for mechanical fixation. This behavior is consistent with typical CubeSat-class structural configurations, demonstrating that the PMU's thermal layout and power density are both reasonable and effective in minimizing component-level thermal drift and oscillations. At the system level, the proposed PMU achieves a balanced design that combines a high degree of integration, a low-noise output, and environmental robustness within the stringent CubeSat-class constraints of smallness and low power budgets. Its multi-output architecture, inrush-current suppression, and health-monitoring mechanisms effectively address key challenges faced by CubeSat-class power systems, including low energy usage, constrained thermal dissipation, and EMC requirements. Relative to conventional single-output CubeSat-class power systems, the presented PMU delivers multiple regulated output rails with smaller power losses, improved fault tolerance, and integrated diagnostic capabilities, thereby improving the overall mission reliability. Nonetheless, investigations into further improvements are warranted. The soft-start circuit can be optimized to increase the stability margins during high-load power-on, and the thermal coupling between the PMU and the metallic baseplate can be improved to reduce the temperature response lag and increase thermal uniformity. These refinements will expand the applications and further improve long-term in-orbit reliability.

To position these results against prior art, Table 4 shows a comparison of the proposed PMU with representative payload-oriented CubeSat-class power studies. Compared with the selected

Table 4
Comparison of the proposed PMU with representative CubeSat-class power studies.

Attribute	This work	Hussein *et al.*(8)	Ali *et al.*(9)	Aburouk *et al.*(12)
Scope	Payload PMU	Modular EPS	CubeSat EPS	DC/DC (LEO)
Regulated output rails	+5 V, ±6 V, ±12 V (incl. isolated)	Multiple	Multiple	Single module
Galvanic isolation	Yes (±12 V)	N/R	N/R	N/R
Inrush suppression	Active soft-start, <420 mA	N/R	N/R	N/R
Health monitoring (V/I/T)	Integrated	Partial	N/R	N/R
Steady-state ripple	≤1.05%	N/R	N/R	N/R
Transient recovery	≈2 μs	N/R	N/R	N/R
Thermal-vacuum validation	−40 to +70 ℃	N/R	N/R	N/R
Average power	≈1.93 W	N/R	N/R	N/R

studies, the present work provides a more complete payload-level validation dataset by combining multi-output regulation, isolated rails, inrush-current suppression, integrated voltage/current/temperature (V/I/T) telemetry, and thermal-vacuum testing within a single prototype. Entries marked "N/R" were not reported in the corresponding sources. It should also be noted that CubeSat-class payload power systems are typically mission-specific rather than general-purpose: their output rails, isolation requirements, and power budgets are dictated by the particular payload. A direct one-to-one comparison of individual performance metrics across studies is therefore of limited value, and Table 4 instead shows a comparison of the designs at the level of architecture and validation scope, which is more meaningful for assessing payload-oriented PMUs than ranking a single figure of merit.

In summary, the proposed PMU exhibits a high degree of integration, excellent stability, and strong environmental robustness, maintaining consistent voltage outputs under vacuum and extreme temperature conditions. This study has not only provided comprehensive experimental data and applied validation methodologies, but has also established a practical technological pathway for the miniaturization and high-reliability design of future small-satellite power management units. This work contributes to the advancement of spaceborne power electronics and improves the practical dependability of CubeSat-class power systems.

6. Conclusions

The design and implementation of a highly integrated, multifunctional PMU developed to address the power requirements of the MPA under the low-power and harsh environmental conditions of CubeSat-class missions have been presented. The proposed PMU integrates multiple key functionalities—including multiple regulated voltage rails, inrush-current suppression, e-Fuse protection, and current and temperature monitoring—to provide a reliable and compact power-distribution solution within strict constraints on size, mass, and power consumption. The system was designed with the aim of ensuring long-term operational stability and electrical safety for satellite payloads.

The comprehensive series of static, dynamic, and environmental validation tests successfully demonstrated the electrical stability and environmental robustness of the proposed PMU. In the static-load tests, all regulated outputs remained within their specified limits, confirming excellent steady-state voltage regulation. In dynamic-load tests, the measured ripple voltages on the +6 and −6 V rails were 63 and 46 mV, respectively, while the transient overshoot was approximately 120 mV, all of which are within the typical noise tolerance of CubeSat-class power systems. The present dynamic-load and ripple characterization focused on the ±6 V signal rails because these are generated by the on-board conversion circuitry designed in this work, whose performance is the subject of this validation. The isolated ±12 V rails, in contrast, are produced by a commercial isolated DC/DC module (MAEU02-HI), whose regulation and ripple are specified and guaranteed by the manufacturer's datasheet; re-characterizing a qualified commercial off-the-shelf (COTS) module falls outside the scope of this work. These isolated rails were confirmed to operate normally, with no anomalies, throughout the thermal-vacuum and radiation tests, and a dedicated load-sweep and isolation-performance characterization is identified as a useful complement for future work. During the verification of inrush-current suppression, the input protection network effectively limited transient surges to below 420 mA, ensuring reliable power-on sequences and the proper activation of the protection mechanism. During the TVC tests, the PMU maintained voltage stability within ±1% across the large temperature range from −40 to +70 °C, with no marked voltage drifts or oscillations. Even under radiative heat dissipation and a measured thermal discrepancy of approximately 20 °C, the system exhibited well-distributed temperature characteristics and stable regulation, demonstrating its capacity for sustained operation in the harsh space environment. Overall, the results reflect a well-balanced PMU design that achieves a high degree of integration, electrical stability, and environmental robustness. Compared with conventional CubeSat-class power systems that provide only a single output or require multiple interconnected converters, the proposed PMU successfully integrates multiple regulated output rails, power-on protection, and health-monitoring mechanisms to improve system reliability and maintainability.

This work has not only provided an experimentally validated reference model for the design of a CubeSat-class power system but has also established a comprehensive verification framework encompassing static- and dynamic-load responses, inrush-current suppression, and thermal-vacuum tests. The proposed methodology can serve as a benchmark for the design and testing of future small-satellite power systems. The initial proton-SEE and ^{60}Co-TID tests reported in Sect. 4.5 further indicate that the payload electronics, including the PMU, tolerated the tested radiation conditions without latch-up, crash, or reboot. Looking forward, comprehensive flight-level radiation qualification—covering a wider range of devices, higher accumulated doses, and heavy-ion SEE characterization—together with long-duration thermal cycling and life-span evaluations, is required to fully verify the long-term reliability of the PMU for use in space missions. In addition, the concept of a smart PMU integrating real-time power monitoring and autonomous load-distribution control can be explored to achieve adaptive power management. The findings of this study provide a solid foundation for the miniaturization and high-reliability design of small-satellite power systems, contributing to the advancement of autonomous and competitive spaceborne power electronics technology. More broadly, by coupling multi-output power delivery with integrated voltage, current, and temperature sensing, the proposed PMU functions as an enabling platform for sensor payloads while itself contributing telemetry suited to AIoT and intelligent-sensing applications, thereby supporting future autonomous health-monitoring and predictive-maintenance capabilities in CubeSat-class missions. Through its integrated temperature sensing (MCP9700), voltage and current monitoring, and the multi-point temperature sensing employed during thermal-vacuum testing, this work is connected to physical-sensor and intelligent-sensing applications; the PMU further serves as the enabling and protection unit for the MPA particle-sensing payload.

Because the present PMU uses COTS devices, the demonstrated results—including the initial radiation tests in Sect. 4.5—should be interpreted as electrical, thermal-vacuum, and preliminary radiation validation rather than complete space qualification. The proton-SEE and ^{60}Co-TID tests showed that the payload, including the PMU, operated without latch-up, crash, or reboot under the tested conditions. For full qualification, radiation-risk mitigation will additionally include component screening based on available radiation data, localized shielding for sensitive analog and switching-control devices, watchdog/reset supervision for telemetry and control electronics, and current-limited e-Fuse isolation to bound latch-up or transient overcurrent events, and more extensive TID and heavy-ion SEE testing remains necessary before flight-level radiation tolerance can be fully claimed.

Although the PMU incorporates EMC-oriented design measures, including galvanic isolation, filtering, and controlled soft-start/inrush-current suppression, formal EMC qualification is being carried out to MIL-STD-461F, as required by the Taiwan Space Agency (TASA). This campaign comprises five major test items, and the scheduled laboratory timeline spans several months; consequently, complete quantitative conducted- and radiated-emission data are not yet available at the time of writing and will be reported once the ongoing tests conclude.

Acknowledgments

The authors would like to thank the Taiwan Space Agency, Taiwan, ROC, for financially supporting this study under grant number TASA-P-1130210. We would like to thank the four anonymous reviewers and the editor for their comments.

References

1 The CubeSat Program: CubeSat Design Specification Rev. 13 (California Polytechnic State Univ., San Luis Obispo, CA, 2014).
2 National Academies of Sciences, Engineering, and Medicine: Achieving Science with CubeSats: Thinking Inside the Box, The National Academies Press, Washington, DC (2016). https://doi.org/10.17226/23503
3 Space News: NASA Venture Class procurement could nurture ride small sat trend (2015).
4 Z. Fang: Sci. Dev. **517** (2016) 60.
5 A. Lotfy, W. Anis, and J. Halim: Proc. 2018 20th Int. Middle East Power Syst. Conf. (MEPCON) (2018) 429. https://doi.org/10.1109/MEPCON.2018.8635169
6 NASA: Small spacecraft technology state-of-the-art, NASA/TP-20210011471 (NASA Ames Res. Center, 2020).
7 NASA: Small spacecraft technology state-of-the-art, NASA/TP-20240013522 (NASA Ames Res. Center, 2024).
8 B. Hussein, A. M. Massoud, and T. Khattab: IEEE Access **10** (2022) 55396. https://doi.org/10.1109/ACCESS.2022.3176902
9 A. Ali, S. A. Khan, M. U. Khan, H. Ali, M. R. Mughal, and J. Praks: Int. J. Aerosp. Eng. **2018** (2018) 2515036. https://doi.org/10.1155/2018/2515036
10 G. Capovilla, F. A. S. Silva, L. M. C. Nascimento, and F. G. C. Leite: Aerospace **7** (2020) 17. https://doi.org/10.3390/aerospace7020017
11 U. Shakoor, M. Alayedi, and E. E. Elsayed: Discov. Energy **5** (2025) 9. https://doi.org/10.1007/s43937-025-00069-5
12 T. Aburouk, S. Kim, H. Masui, and M. Cho: J. Small Satell. **7** (2018) 701.
13 R. H. G. Chacón, A. V. Dias, and S. Finco: Analog Integr. Circuits Signal Process. **112** (2022) 289. https://doi.org/10.1007/s10470-022-02041-y
14 A. Cervone, F. Topputo, V. Franzese, A. Rodríguez Pérez-Silva, B. Benavent Leon, B. Delmas Garcia, P. Minacapilli, P. Rosa, G. Bay, and S. Radu: CEAS Space J. **16** (2023) 203. https://doi.org/10.1007/s12567-023-00517-9
15 J. Bouwmeester, A. Menicucci, and E. K. A. Gill: Reliability Eng. Syst. Saf. **220** (2022) 108288. https://doi.org/10.1016/j.ress.2021.108288
16 M. Eilenberger, H. Gunasekar, D. G. Toro, and C. Bänsch: CEAS Space J. **16** (2024) 1. https://doi.org/10.1007/s12567-023-00526-8

17 A. González-Llana, L. Peinado-Pérez, E. Roibás-Millán, J. Pérez-Álvarez, I. Torralbo-Gimeno, and A. Gómez-San-Juan: Proc. 8th Eur. Conf. for Aeronaut. Space Sci. (EUCASS) (2019). https://doi.org/10.13009/EUCASS2019-842
18 J. N. Buitrago-Leiva, I. Terraza-Palanca, L. Contreras-Benito, L. Fernandez, G. Gracia-Sola, C. del Castillo Sancho, L. Ha, D. Palma, M. Solyga, and A. Camps: Aerospace **11** (2024) 805. https://doi.org/10.3390/aerospace11100805
19 Y. G. Lv, Y. T. Wang, T. Meng, Q. W. Wang, and W. X. Chu: Green Energy Intell. Transp. **3** (2024) 153. https://doi.org/10.1016/j.enss.2024.03.001

About the Authors

Yung-Tsung Cheng received his B.S. degree from the Department of Electronic Engineering, Kun Shan University, Tainan, Taiwan in 2011, M.S. degree from the Department of Electronic Engineering, Kun Shan University, Tainan, Taiwan, in 2013, and Ph.D. degree from the Department of Electrical Engineering, National Cheng Kung University, Tainan City, Taiwan, in 2023. Since 2025, he has been an assistant professor at the Department of Electric Vehicles and Intelligent Electronics, Kun Shan University. His research interests are in medical technology aids, electronic instrumentation system, automation control, ROS robot applications, and system integration. (520.yong.cong@gmail.com)

Tzu-Fang Chang received her Ph.D. degree from National Cheng Kung University, Taiwan. She is presently an assistant professor at the Institute of Space and Plasma Sciences, National Cheng Kung University, Taiwan. Her research interests are in space physics and space instrument development. (jocelyn@pssc.ncku.edu.tw)

Chih-Yu Chiang received his Ph.D. degree from National Cheng Kung University (NCKU), Taiwan. Currently, he is a postdoctoral researcher at the Center for Advanced Plasma Science and Technology, NCKU, Taiwan. His research interests are in space science and the development of space instruments. (johnson@pssc.ncku.edu.tw)

Yu-Rong Cheng received his B.S. degree from National Ilan University (NIU) in Taiwan and M.S. degree from National Cheng Kung University (NCKU), also in Taiwan. He is currently pursuing his Ph.D. degree in electrical engineering at NCKU. His research interests are in space science and the development of space instruments. (LA6101042@gs.ncku.edu.tw)

Cheng-Chi Tai received his B.S. degree from the Department of Electronic Engineering, Chung Yuan Christian University, Taoyuan City, Taiwan, in 1986, M.S. degree from the Department of Electrical Engineering, National Cheng Kung University, Tainan City, Taiwan, in 1988, and Ph.D. degree from Iowa State University, Ames, USA, in 1997. From 1990 to 1992, he was an assistant professor at Kun Shan University, Tainan City, Taiwan. Since 1997, he has been a professor at the Department of Electrical Engineering, National Cheng Kung University, Tainan City, Taiwan. His research interests are in bio-electronic instrumentation system, electromagnetic testing, pulsed eddy current, photoinductive imaging ultrasound, acoustic emission, and biomedical image/signal processing. (ctai@mail.ncku.edu.tw)